

Rine, *EMBO J.* **7**, 2241 (1988).

6. F. J. McNally and J. Rine, *Mol. Cell. Biol.* **11**, 5648 (1991).
7. J. Abraham, K. A. Nasmyth, J. N. Strathern, A. J. Klar, J. B. Hicks, *J. Mol. Biol.* **176**, 307 (1984); J. B. Feldman, J. B. Hicks, J. R. Broach, *ibid.* **178**, 815 (1984).
8. D. H. Rivier and J. Rine, *Science* **256**, 659 (1992); unpublished data.
9. A. M. Miller and K. A. Nasmyth, *Nature* **312**, 247 (1984).
10. S. P. Bell, J. Mitchell, J. Leber, R. Kobayashi, B. Stillman, *Cell* **83**, 563 (1995).
11. C. T. Chien, S. Buck, R. Sternglanz, D. Shore, *ibid.* **75**, 531 (1993).
12. A *GAL4-SIR1* fusion gene was set under control of the constitutive promoter of the yeast alcohol dehydrogenase I, *ADH1p* [G. Ammerer, *Methods Enzymol.* **101**, 192 (1983)] in pRS316 (31). The *GAL4-SIR1* fusion plasmid (pCF117) contained *ADH1p* (Bam HI–Hind III from pJR1208), followed by *GAL4-SIR1* (Hind III–Bgl II from pKL5 [C. Chien, P. L. Bartel, R. Sternglanz, S. Fields, *Proc. Natl. Acad. Sci. U.S.A.* **88**, 9578 (1991)] containing the 5' end of the gene) and the 3' end of *SIR1* including the *SIR1* terminator (Bgl II–Hind III from pJR979).
13. Gal4 binding sites were introduced in place of the ACS of the synthetic *HMR* silencer (6). First, a Bam HI–Sph I fragment containing the ACS was excised from pJR1273. pJR1273 consisted of the Eco RI–Hind III fragment of *HMR* cloned into the Eco RI–Hind III sites of pUC18. This *HMR* allele also lacked *HMR-I*. In place of the excised ACS, annealed nucleotides that formed the Gal4 binding site were inserted (5'-GATCCCCCTCGAGGATCTCGGAAGACTCTCC-TCCGGCTGATGCATG-3'). Plasmids were screened for multiple insertions, and isolates that had one, three, and five tandem insertions (pJR1584, pJR1614, and pJR1619, respectively) were used to replace the *hmrΔ::URA3* allele in JRY3933 (*MATα ade2-1 his3-11,15 leu2-3,112 trp1-1 ura3-1 can1-100 hmrΔ::URA3*) by one-step gene replacement [R. J. Rothstein, *Methods Enzymol.* **101**, 202 (1983)]. Correct integration was verified by DNA blot hybridization.
14. C. Fox, S. Loo, J. Rine, data not shown.
15. B. F. Pugh and R. Tjian, *Cell* **61**, 1187 (1990); *Genes Dev.* **5**, 1935 (1991); B. P. Cormack and K. Struhl, *Science* **262**, 244 (1993).
16. A methionine-regulated *GAL4-SIR1* fusion gene was obtained by inserting the Hind III fragment of pCF117 into Hind III-linearized pJR1588. pJR1588 is a derivative of pRS313 (31), which carries a Sal I–Eco RV fragment of the *ME73* promoter [H. Cherest, P. Kerjan, K. Y. Surdin, *Mol. Gen. Genet.* **210**, 307 (1987)] inserted at Xho I–Eco RV.
17. L. H. Hartwell, *J. Mol. Biol.* **104**, 803 (1976).
18. C. W. Jacobs, A. E. Adams, P. J. Szanislo, J. R. Pringle, *J. Cell Biol.* **107**, 1409 (1988).
19. F. Felici, G. Cesareni, J. M. X. Hughes, *Mol. Cell. Biol.* **9**, 3260 (1989).
20. T. Triolo and R. Sternglanz, *Nature* **381**, 251 (1996).
21. To create the Gal4-Orc2 and Gal4-Orc5 fusion proteins, we amplified the *ORC2* and *ORC5* open reading frames from yeast genomic DNA by polymerase chain reactions (PCR). The PCR primers used introduced Bam HI sites both 5' and 3' of both genes. The PCR products were cleaved with Bam HI and ligated into the Bam HI site of pRH98-1, thus setting them under control of the constitutive glyceraldehyde dehydrogenase (GPD) promoter and the phosphoglycerate kinase (PGK) terminator. pRH98-1 is a derivative of YCplac33 [R. D. Gietz and A. Sugino, *Gene* **74**, 527 (1988)], which has the Hind III–Xba I fragment of pG-1 [M. Schena, D. Picard, K. R. Yamamoto, *Methods Enzymol.* **194**, 389 (1991)] containing a GPD-PGK cassette inserted at the Hind III and Xba I sites. The resulting plasmids, pJR1637 (expressing *ORC2*) and pJR1638 (expressing *ORC5*), were able to complement the temperature sensitivity and silencing defect of *orc2-1* and *orc5-1*, respectively. Subsequently, a derivative of pRH98-1 was constructed that encoded the Gal4 DNA binding domain (residues 1 to 147). The *GAL4* sequence was obtained by PCR amplification from yeast

genomic DNA. The primers were designed such that a Bgl II site was generated 5' and a Bam HI site was created 3' of the *GAL4* sequence. The PCR product was cleaved with Bgl II and Bam HI and inserted into the Bam HI site of pRH98-1, between *GPDp* and *PGK*, generating pJR1639. Bam HI fragments containing *ORC2* (pJR1637) and *ORC5* (pJR1638) were cloned into the unique Bam HI site of pJR1639, generating the Gal4(1–147)-Orc2 (pJR1640) and Gal4(1–147)-Orc5 (pJR1641) fusion plasmids.

22. J. Zhu, C. S. Newlon, J. A. Huberman, *Mol. Cell. Biol.* **12**, 4733 (1992).
23. O. M. Aparicio, B. L. Billington, D. E. Gottschling, *Cell* **66**, 1279 (1991).
24. D. E. Gottschling, O. M. Aparicio, B. L. Billington, V. A. Zakian, *ibid.* **63**, 751 (1990).
25. D. D. Dubey *et al.*, *Mol. Cell. Biol.* **11**, 5346 (1991).
26. O. M. Aparicio and D. E. Gottschling, *Genes Dev.* **8**, 1133 (1994).
27. A. Axelrod and J. Rine, *Mol. Cell. Biol.* **11**, 1080 (1991).
28. D. S. Henderson, S. S. Banga, T. A. Grigliatti, J. B. Boyd, *EMBO J.* **13**, 1450 (1994).

29. A. Hecht, T. Laroche, S. Strahl-Bolsinger, S. M. Gasser, M. Grunstein, *Cell* **80**, 583 (1995); A. Hecht, S. Strahl-Bolsinger, M. Grunstein, *Nature* **383**, 92 (1996).
30. F. Palladino *et al.*, *Cell* **75**, 543 (1993).
31. R. S. Sikorski and P. Hieter, *Genetics* **122**, 19 (1989).
32. B. J. Brewer and W. L. Fangman, *Cell* **51**, 463 (1987).
33. We thank D. Gottschling for constructs and the members of our laboratory for stimulating discussions. Supported by a grant from the National Institutes of Health (GM31105) (J.R.), by postdoctoral fellowships from the California Division of the American Cancer Society and the Leukemia Society of America (C.A.F.), by postdoctoral grants from the Swiss National Science Foundation and the Janggen-Pöhn Foundation (A.E.E.-M.), and by a Howard Hughes Medical Research Institute predoctoral fellowship (S.L.). C.A.F. thanks M. D. Sheets for discussion and support. Core support was provided by a National Institute of Environmental Health Sciences Mutagenesis Center grant to B. N. Ames.

14 August 1996; accepted 11 April 1997

Orientation Selectivity in Pinwheel Centers in Cat Striate Cortex

Pedro E. Maldonado,*† Imke Gödecke,* Charles M. Gray, Tobias Bonhoeffer

In primary visual cortex of higher mammals neurons are grouped according to their orientation preference, forming “pinwheels” around “orientation centers.” Although the general structure of orientation maps is largely resolved, the microscopic arrangement of neuronal response properties in the orientation centers has remained elusive. The tetrode technique, enabling multiple single-unit recordings, in combination with intrinsic signal imaging was used to reveal the fine-grain structure of orientation maps in these locations. The results show that orientation centers represent locations where orientation columns converge containing normal, sharply tuned neurons of different orientation preference lying in close proximity.

In recent years, optical imaging has enabled the investigation of neuronal response properties over large areas of the visual cortex in vivo (1–3). These experiments have revealed that orientation selectivity is not organized in parallel bands but in iso-orientation domains that are arranged radially in a pinwheel-like fashion (4). Optical imaging studies have shown that the magnitude of the orientation signal in the centers of these pinwheels is low (1, 3, 4), suggesting that the population of neurons in these locations might mainly consist of unoriented cells. However, be-

cause of their relatively low spatial resolution, imaging studies cannot reliably determine the physiological characteristics of individual neurons in these regions. We have previously reported that in some locations of cat striate cortex, adjacent cells display large differences in orientation preference (5). Because this is an alternative explanation for the low magnitude of the optical orientation signal, we conjectured that these regions may correspond to the pinwheel centers in the orientation preference map.

In five halothane-anesthetized adult cats, we used optical imaging based on intrinsic signals to record the orientation preference maps of visual areas 17 and 18 (6). The animals were stimulated with drifting square wave gratings of different orientations. The image of the visual cortical surface obtained in one experiment along with the corresponding “angle” and “polar” maps is shown in Fig. 1 (7). After obtaining these maps, we used tetrodes, which enable simultaneous and separable recording of small numbers of neighbouring neurons (8,

P. E. Maldonado, Max-Planck-Institute for Psychiatry, Am Klopferspitz 18A, 82152 München-Martinsried, Germany, and The Center for Neuroscience, University of California, Davis, CA 95616, USA.

I. Gödecke and T. Bonhoeffer, Max-Planck-Institute for Psychiatry, Am Klopferspitz 18A, 82152 München-Martinsried, Germany.

C. M. Gray, The Center for Neuroscience and the Section of Neurobiology, Physiology and Behavior, University of California, Davis, CA 95616, USA.

*These authors contributed equally to the work.

†To whom correspondence should be addressed at The Center for Neuroscience, University of California, Davis, CA 95616, USA. E-mail: pedro@chaos.ucdavis.edu

9), to record from pinwheel centers or iso-orientation domains while presenting the same drifting square wave gratings used in the imaging session. Subsequently, we extracted and sorted the individual spike trains from the multi-unit recording, computed peri-stimulus time histograms (PSTHs) and tuning curves for all cells (9, 10), and compared the response properties

for neurons within and outside of orientation centers.

In 24 penetrations in pinwheel centers, we recorded at 77 sites and extracted a total of 345 single neurons (Table 1). As a control, we performed 20 penetrations in iso-orientation domains (11) yielding 81 sites and a total of 348 neurons. By statistically comparing the firing rate before and during

stimulus presentation, we found 8% of the cells in pinwheel centers and 7% of the cells in iso-orientation domains to be unresponsive to the presented stimuli. Fourteen percent of the cells in pinwheel centers and 17% in iso-orientation domains were not tuned (12). For the remaining tuned cells, tuning bandwidths and firing rates were determined and were indistinguishable be-

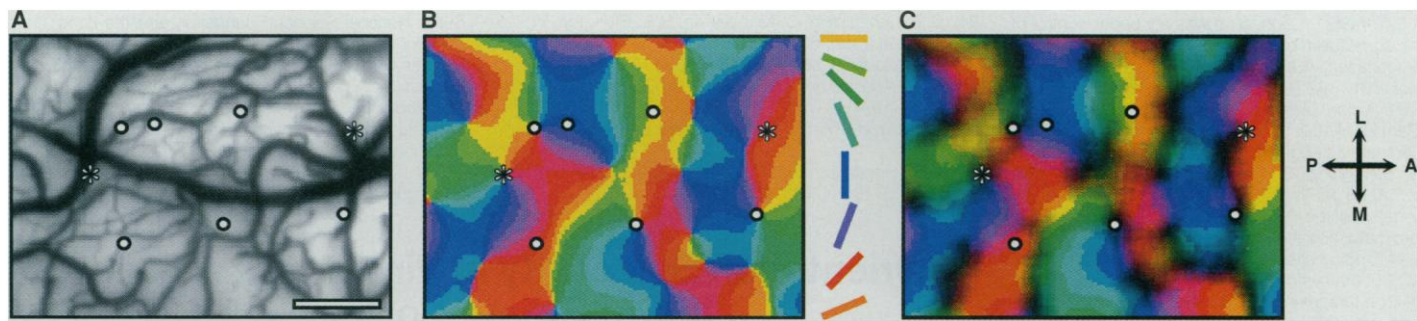


Fig. 1. Orientation map obtained by intrinsic signal imaging. **(A)** Vascular pattern of the cortical surface. This area contains portions of visual areas 17 and 18. The circles in the panels show the locations of the tetrode penetrations. These penetrations were aimed at orientation centers or at iso-orientation domains [see **(B)**]. The two asterisks indicate the locations of the recordings shown in Fig. 2. Scale bar, 1 mm. **(B)** Color-coded orientation preference (“angle”) map for the cortical region shown in **(A)**. The responses to four stimulus orientations were summed vectorially, and the preferred orientation for every point is color-coded as shown on the right. This angle map reveals the

typical organization of orientation preference maps into pinwheel centers (where different orientation preferences converge; for example, left asterisk) and iso-orientation domains (where neurons of similar orientation preference are grouped together; for example, right asterisk). **(C)** Polar map, combining the color code for preferred orientation with a brightness code representing the strength of orientation tuning [for details see (3, 4, 16)]. Dark regions represent areas of weak tuning, whereas bright areas represent strong orientation preference. Note that dark areas are prevalent in pinwheel centers (for instance, middle circle lower row). L, lateral; M, medial; P, posterior; and A, anterior.

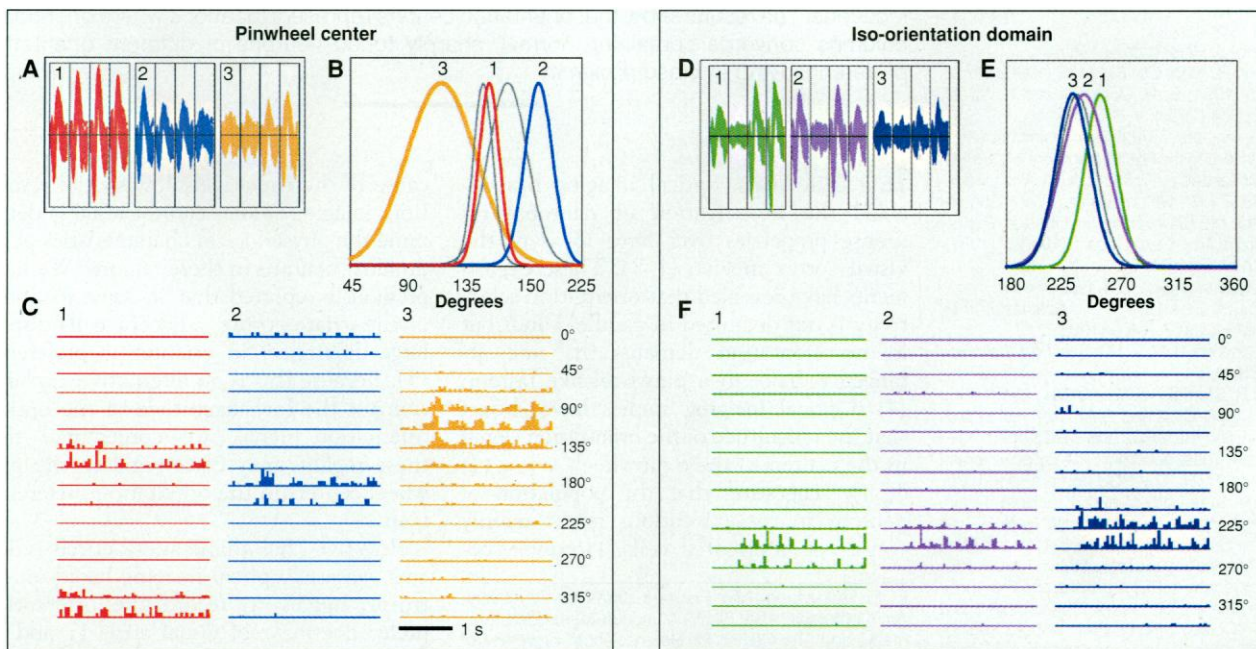


Fig. 2. Examples of response properties of single units recorded at the center of a pinwheel **(A to C)** and in the middle of an iso-orientation domain **(D to F)**. **(A)** and **(D)** depict data from three neurons. For each neuron 50 superimposed waveforms recorded from the four wires of the tetrode are shown separately. Note that the pattern of spike amplitudes across the four channels varies from cell to cell. **(B)** and **(E)** show tuning curves [Gaussian fit (10)] from recordings in a pinwheel center and an iso-orientation domain. Numbers (1, 2, and 3) and colors label tuning curves from cells whose spike-waveforms **(A)** and **(D)** and PSTHs **(C)** and **(F)** are shown in the other panels. Unlabeled, gray curves represent neurons from the

same recording site that were simultaneously recorded but not displayed further. **(C)** and **(F)** are peristimulus time histograms for the same three neurons shown in **(A)** and **(D)**. The cells were stimulated by monocular presentation of an oriented drifting square wave grating. Each row corresponds to the cell’s response to a different stimulus orientation ranging from 0° to 360° in 22.5° steps. In this example, neurons from the pinwheel center **(A)** to **(C)** exhibit wide variance in orientation preferences (orientation scatter: 22.6°, orientation range: 70°), whereas cells from the iso-orientation domain **(D)** to **(F)** show small variance (orientation scatter, 12.3°; orientation range, 29°).

tween orientation centers and iso-orientation domains (Table 1). This finding demonstrates that neurons in pinwheel centers are as selective for stimulus orientation as those in other locations of the cortex and that pinwheel centers do not contain larger populations of unselective cells, as might be inferred from the reduced brightness of the polar maps characteristic for these locations.

One implication of this finding is that pinwheel centers would be expected to show greater local variance in orientation preference than iso-orientation domains. Using circular statistics, we defined the measures of orientation scatter and orientation range (13) and found, as expected, that both measures were significantly larger for sites recorded in pinwheel centers than for sites recorded in iso-orientation domains (Table 1).

This result is further illustrated by Fig. 2, which displays the response properties of a group of cells recorded from a pinwheel center (panels A, B, and C) and another group in an iso-orientation domain (panels D, E, and F). These plots show that the neurons recorded from the pinwheel center are indeed tuned to widely different orientations (orientation range 70° in Fig. 2, A to C), whereas the cells recorded in the iso-orientation domain are tuned to similar orientations (and directions). This is most clearly visible in panels B and E of Fig. 2 where Gaussian fits of the orientation tuning curves for each of the cells are shown (10).

Occasionally, we found sites within iso-orientation domains that displayed an unexpectedly large orientation scatter (14). These data seem to be at odds with the

optical imaging data where iso-orientation domains are represented as regions with a homogeneous population of neurons with similar orientation tuning. However, optical imaging based on intrinsic signals mainly records neuronal activity from cells lying less than 600 to 800 μm below the cortical surface (15, 16). Therefore, to compare directly the optical and electrophysiological recordings, we determined the orientation scatter as a function of the recording depth (Fig. 3). In the case of the pinwheel centers there is no trend of the orientation scatter to change with increasing depth. In contrast, in iso-orientation domains a linear regression shows a significant ($P < 0.05$) positive slope, indicating that in this case orientation scatter continuously increases with depth. Consequently, if only data obtained from sites located in the upper 700

Table 1. Statistics for all the data and for a subset sampled from upper cortical layers (above 700 μm) grouped by recording locations in pinwheel centers and iso-orientation domains. The Kolmogorov-Smirnov (KS) test was used to determine if the two samples were derived from the same population with respect to tuning bandwidth and firing rate. All values are well above 0.05, indicating that even this sensitive test cannot detect differences between the two samples. The *t* test (two-tailed; TT) was used to prove that the two samples significantly ($P < 0.01$) differ in orientation scatter and orientation range. Because here the scatter of the different parameters within the populations is the relevant entity, standard deviations (which describe this scatter) are used rather than standard errors of the mean (which describe the precision of the measurement of the population's mean).

Statistic parameters	Pinwheel centers	Iso-orientation domains	Significance (<i>P</i> value)
<i>Group data</i>			
Number of cells	345	348	
Unresponsive	28	25	
Untuned	48	59	
Tuned	269	264	
Mean tuning bandwidth of tuned cells (degrees)	31.3 ± 17.6	28.3 ± 16.7	0.10 (KS)
Mean firing rate to optimal stimulus (spikes/s)	21.9 ± 24.7	19.3 ± 26.3	0.37 (KS)
Number of sites with more than one tuned cell/total number of sites	63/77	68/81	
Mean orientation scatter* (degrees)	18.8 ± 11.2	13.8 ± 9.8	0.0092 (TT)
Mean orientation range† (degrees)	40.5 ± 24.6	28.3 ± 19.6	0.0024 (TT)
Sites with orientation range >60°	14	5	
<i>Data from cortical depth less than ~700 μm</i>			
Number of cells	183	152	
Unresponsive	13	10	
Untuned	24	13	
Tuned	146	129	
Mean tuning bandwidth of tuned cells (degrees)	28.2 ± 15.4	26.4 ± 18.0	0.15 (KS)
Mean firing rate to optimal stimulus (spikes/s)	19.5 ± 20.5	19.2 ± 23.4	0.96 (KS)
Number of sites with more than one tuned cell/total number of sites	35/43	34/35	
Mean orientation scatter* (degrees)	18.5 ± 12.4	10.7 ± 6.3	0.0017 (TT)
Mean orientation range† (degrees)	39.2 ± 26.6	22.8 ± 14.4	0.0024 (TT)
Sites with orientation range >60°	8	1	

*Orientation scatter: standard deviation of orientations within one recording site. †Orientation range: smallest arc containing all data points.

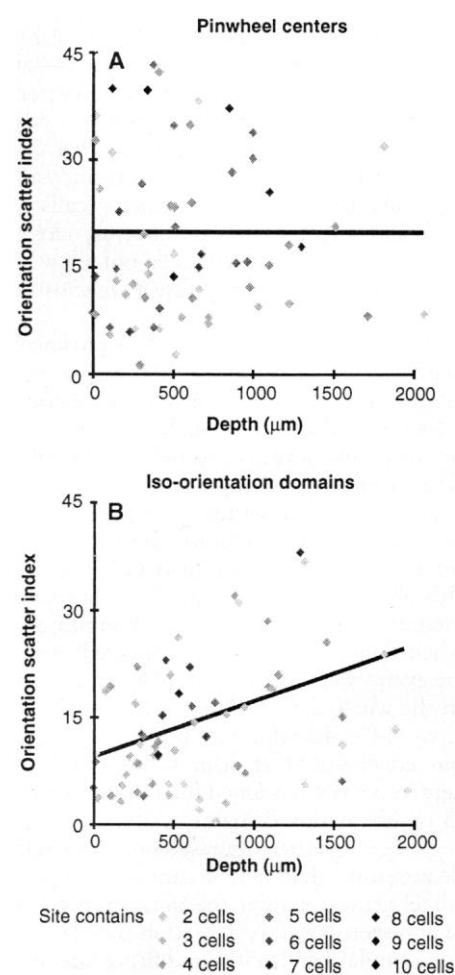


Fig. 3. Orientation scatter in pinwheel centers (A) and iso-orientation domains (B) as a function of depth. The orientation scatter at each site is plotted against cortical depth. The gray scale of the squares (see bottom of the figure) codes for the number of neurons that contributed to the data point. For the calculation of the regression line, the contribution of each data point was weighted according to the number of neurons sampled.

μm are considered (17), the difference in orientation scatter between pinwheel centers and iso-orientation domains becomes much more pronounced than if the comparison is made for the complete data set (Table 1). Similarly, another related measure clearly reveals a difference between pinwheel centers and iso-orientation domains (Table 1): especially in the upper 700 μm of the cortex, the percentage of sites in which the orientation range exceeds 60° is much larger in pinwheel centers (23%) than in iso-orientation domains (3%).

Our observation that orientation scatter increases with cortical depth in iso-orientation domains could have at least two explanations: First, it could reflect a true increase in the heterogeneity of orientation tuning in deep layers of cortex. This is supported by some earlier single-unit studies which also reported that orientation scatter increases with cortical depth (18). Alternatively, the strong curvature of the imaged cortical region on the lateral gyrus might account—at least in part—for the larger orientation scatter in deeper layers. Assuming a strictly columnar arrangement, it is likely that columnar width would decrease with increasing cortical depth, thereby placing cells of different orientation preference in closer proximity. The present data do not allow us to distinguish between these two possible explanations.

For the recordings targeted at pinwheel centers, it could be argued that, despite our effort to hit these locations, we were slightly off-target and missed a small population of untuned cells located precisely in the pinwheel centers. One way to address this concern is to score only those sites as successful pinwheel penetrations in which we found an orientation range larger than 60° , because this should only occur in the immediate vicinity of pinwheel centers. Interestingly, when only these data are considered, there are even fewer untuned cells (4%; 3/72) than in the whole data set for pinwheel penetrations (14%; 48/345). This further reinforces our conclusion that neurons in pinwheel centers are not less tuned than those located in iso-orientation domains.

Taken together the results of this study demonstrate that neurons in or near pinwheel centers exhibit the same proportion of unresponsive and orientation-tuned cells, have similar bandwidths and firing rate distributions, and are thus as selective for stimulus orientation as neurons in iso-orientation domains. Thus, the regions of reduced brightness in the polar maps, characteristic for pinwheel centers, do not reflect a lack of neuronal orientation selectivity, but rather result from the summation of cellular responses with greater variance in orientation preference.

These results differ from predictions made by some models of orientation preference that assume orientation centers as regions of decreased orientation selectivity [see, for example, (19)]. Our data suggest that pinwheel centers, with respect to orientation preference, do not represent functionally distinct compartments within striate cortex: Their orientation-tuning properties appear to be indistinguishable from those of iso-orientation domains. This has important implications for cortical organization. It means that the anatomical connectivity of pinwheel centers requires a remarkable degree of specificity. If orientation selectivity arises by the alignment of thalamic afferents (20), the thalamocortical projections into pinwheel centers will require a much higher degree of precision than similar projections into iso-orientation domains. By the same token, if cortico-cortical connections projecting to pinwheel centers link regions of similar orientation preference (21), they would require substantially more accuracy than those projecting to iso-orientation domains. It is remarkable that developmental mechanisms seem to be able to provide this degree of topographic precision for setting up the neural network of the visual cortex.

REFERENCES AND NOTES

- G. G. Blasdel and G. Salama, *Nature* **321**, 579 (1986).
- A. Grünvald, E. E. Lieke, R. D. Frostig, C. D. Gilbert, T. N. Wiesel, *ibid.* **324**, 361 (1986).
- D. Y. Ts'o, R. D. Frostig, E. E. Lieke, A. Grünvald, *Science* **249**, 417 (1990).
- T. Bonhoeffer and A. Grünvald, *Nature* **353**, 429 (1991); *J. Neurosci.* **13**, 4157 (1993).
- P. E. Maldonado and C. M. Gray, *Visual Neurosci.* **13**, 509 (1996).
- All experiments followed local and National Institutes of Health (NIH) guidelines for the care and use of laboratory animals. After initial anesthesia (mixture of ketamine and xylazine), young adult cats (1.5 to 2.5 kg) were ventilated by using halothane (0.6 to 1.5%) as an anesthetic in a mixture of nitrous oxide and oxygen (2:1). Electrocardiogram, electroencephalogram, arterial oxygen saturation (SpO_2), expired CO_2 , and rectal temperature were continuously monitored. The skull was opened above areas 17 and 18, and a titanium chamber was implanted, filled with silicon oil, and closed with a glass cover slip (16). After the surgery, the animals were paralyzed with succinylcholine hydrochloride (20 mg per kilogram of body weight per hour) administered in Ringer solution containing 5% dextrose (4 ml/kg per hour). Details of the optical imaging procedures can be found in (4, 16). Briefly, the cortical surface was illuminated with light of 707-nm wavelength, and the animal was presented with moving square wave gratings (0.3 to 1 cycle per degree) of four different orientations, back-projected onto a translucent frosted-glass screen covering 60° of visual angle, located 1 m in front of the animal. The eyes were focused on the tangent screen with an appropriate pair of contact lenses. Images were acquired from the exposed part of the cortex with a slow-scan charge-coupled device camera (ORA 2001, Optical Imaging, Germantown, NY).
- Activity maps were calculated by dividing the images obtained for one orientation by the sum of the images obtained for all orientations or "cocktail blank" (4, 16). Angle maps were computed by summing the responses to all stimulus orientations for each pixel vectorially, taking the magnitude of the responses as vector lengths and the stimulus orientation as vector angles, and plotting the vector angle with a discrete pseudocolor code. In polar maps the magnitude of the resulting vector is additionally displayed as the brightness of the color at the respective pixel, constituting a measure of the sharpness in orientation tuning of the respective cortical location (4, 16).
- M. A. Wilson and B. L. McNaughton, *Science* **261**, 1055 (1993); C. M. Gray, P. E. Maldonado, M. A. Wilson, B. L. McNaughton, *J. Neurosci. Methods* **63**, 43 (1995). The recorded cells are estimated to lie within a spherical volume of tissue with an approximate radius of 65 μm .
- Tetrode fabrication and recording methods are described in (8). For each of the different data sets, spike separation was achieved by an interactive computer program. Action potentials arising from geniculate fibers and axons of passage were excluded from our sample on the basis of their distinct wave form. From the individual spike trains, orientation-tuning curves were constructed on the basis of mean firing rate over all trials during the presentation of the stimulus and the cell's spontaneous activity. The stimuli were the same as for the imaging session except that stimulation was monocular with eight different orientations and two directions of motion. For each point in a tuning curve, the mean and standard deviation was calculated. To determine if a particular cell was responsive to the stimulus, we performed a Student's *t* test between the peak value of the tuning curve and its corresponding value of spontaneous activity.
- We fitted a Gaussian function to the tuning curve using the maximum likelihood method [G. H. Henry, B. Dreher, P. O. Bishop, *J. Neurophysiol.* **34**, 1394 (1974)]. In each fit, the χ^2 represents the statistical measure of the difference between the experimental data and the Gaussian. From the Gaussian fit of each cell, we estimated the orientation preference (peak) and the orientation bandwidth (σ of Gaussian). In the case of nondirectional cells, the Gaussians were always fit to the higher of the two peaks. Orientation preference was used modulo 180° for determining orientation scatter and orientation range [see (13)].
- These penetrations were aimed at regions where the orientation signal was strong (that is, where colors in the polar map were bright). Whenever possible we tried to exclude "saddle points" (where the progression of orientation values reverses). Although orientation preference in saddle points generally changes more slowly, these locations were avoided, because they are singular points in the orientation preference map and are thus not representative for iso-orientation domains.
- To determine if cells were tuned to the stimuli, we compared the Gaussians fit's χ^2 to that of a fit to a straight line at the mean amplitude level of the same tuning curve. The arithmetic difference between both χ^2 's is also distributed as χ^2 . Thus, significant differences ($P < 0.01$) reflect a better fit of the data to a Gaussian curve than to a linear function [see K. H. Britten, M. N. Shadlen, W. T. Newsome, J. A. Movshon, *J. Neurosci.* **12**, 4745 (1992)]. In those cases where the Gaussian function showed a significant lack of fit [$P > 0.01$; χ^2 test (10)], or where the Gaussian fit was not significantly better than the linear fit to the mean firing rate, the cells were considered untuned for orientation.
- We used circular statistics [for example, E. Batschelet, *Circular Statistics in Biology* (Academic Press, New York, 1991)] to assess the variance in orientation preference for the different recording sites. Using vectorial addition, we computed the mean and standard deviation of the orientation preferences of all cells at each site. The standard deviation constitutes a measure of the orientation scatter, which has the virtue of being independent from the number of cells recorded at each site. Its magnitude reflects the variability of orientation preference among all tuned cells at each site. The orientation range, defined as the smallest arc containing all orientation preferences, was also used for quantification.

14. Assuming a hypercolumn spacing of 1 mm, it follows that two cells separated maximally in our tetrode recordings [$\sim 130 \mu\text{m}$ (8)] should exhibit an orientation preference difference no larger than 23° , with the majority yielding correspondingly smaller values. Yet in iso-orientation domains, there was a substantial number of cell pairs (28%) whose orientation preference differed by more than 23° .
15. D. Malonek, D. Shoham, E. H. Ratzlaff, A. Grinvald, *Soc. Neurosci. Abstr.* **130**, 4 (1990).
16. T. Bonhoeffer and A. Grinvald, in *Brain Mapping: The Methods*, A. Toga and J. C. Mazziotta, Eds. (Academic Press, San Diego, CA, 1996), pp. 55–97.
17. We included all the data acquired during the first 500

- μm of each penetration and arbitrarily defined zero depth as the location where we first encountered neuronal activity. Because the first cells are typically encountered $\sim 200 \mu\text{m}$ into the cortex, a depth of $500 \mu\text{m}$, according to our definition, corresponds to an absolute depth of $\sim 700 \mu\text{m}$.
18. D. H. Hubel and T. N. Wiesel, *J. Physiol.* **165**, 559 (1963); B. B. Lee, K. Albus, P. Heggelund, M. J. Hulme, O. D. Creutzfeldt, *Exp. Brain Res.* **27**, 301 (1977).
19. N. V. Swindale, *Network Comput. Neural Sys.* **7**, 161 (1996).
20. D. H. Hubel and T. N. Wiesel, *J. Physiol.* **160**, 106 (1962); B. Chapman, K. R. Zahs, M. Stryker, *J. Neurosci.* **11**, 1347 (1994); R. C. Reid and J. M. Alonso, *Nature* **378**, 381 (1995); D. Ferster, S. Chung, H. Wheat, *ibid.* **380**, 249 (1996).
21. C. D. Gilbert and T. N. Wiesel, *J. Neurosci.* **9**, 2432 (1989).
22. We thank F. Brinkmann for technical help and M. Hübener and K. Britten for helpful comments on earlier versions of the manuscript. This work was supported by the Max-Planck Gesellschaft, by a grant from the National Eye Institute to C.M.G., and fellowships from the McDonnell-Pew Foundation to P.E.M. and the Klingenstein Fund to C.M.G.

31 January 1997; accepted 16 April 1997

Genetic Feminization of Pheromones and Its Behavioral Consequences in *Drosophila* Males

Jean-François Ferveur,* Fabrice Savarit, Cahir J. O’Kane, Gilles Sureau, Ralph J. Greenspan,† Jean-Marc Jallon

Pheromones are intraspecific chemical signals important for mate attraction and discrimination. In the fruit fly *Drosophila melanogaster*, hydrocarbons on the cuticular surface of the animal are sexually dimorphic in both their occurrence and their effects: Female-specific molecules stimulate male sexual excitation, whereas the predominant male-specific molecule tends to inhibit male excitation. Complete feminization of the pheromone mixture produced by males was induced by targeted expression of the *transformer* gene in adult oenocytes (subcuticular abdominal cells) or by ubiquitous expression during early imaginal life. The resulting flies generally exhibited male heterosexual orientation but elicited homosexual courtship from other males.

In many animal species, sex- and species-specific bouquets of odors elicit subtle changes in potential sexual partners, which in turn may respond by appropriate behavior (1). In the fruit fly *Drosophila*, the stereotyped courtship behavior exhibited by male flies is induced largely by chemical cues, or pheromones, produced by his mate (2). These pheromones—the most abundant hydrocarbon molecules present on the fly cuticle (3)—are sensed principally by contact and are thought to play a crucial role in sexual isolation, tending to prevent interspecific mating (4, 5).

In *D. melanogaster*, pheromones are strikingly sexually dimorphic (6) and have very different effects on male courtship behavior (7, 8) (Table 1). Female flies produce dienes (two double bonds) with 27 and 29 carbons [*cis,cis*-7,11-heptacosadiene (7,11HD) and *cis,cis*-7,11-nonacosadiene (7,11ND)]. A few tens of nanograms of both dienes together

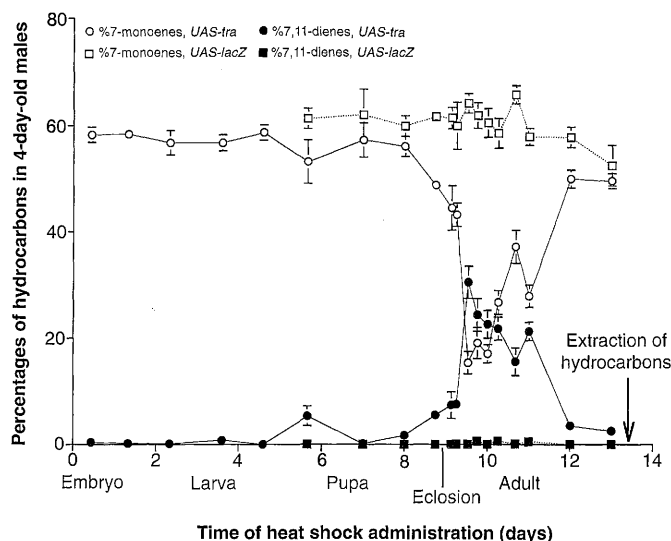
can elicit vigorous male precopulatory behavior (7, 8). Male flies synthesize monoenes (one double bond) with 23 and 25 carbons [*cis*-7-tricosene (7-T) and *cis*-7-pentacosene (7-P)]. 7-T can inhibit dose-dependent male excitation (8, 9), whereas 7-P stimulates males of some strains (4, 7, 8).

One of the few genetic factors known to control the production of sex pheromones in

D. melanogaster (10, 11) is the gene *transformer* (*tra*), which controls the sexual dimorphism of pheromones (8, 12) as part of its larger influence on somatic sex determination. When the feminizing transgene *UAS-tra*, made with the female cDNA of the *tra* gene, is expressed in certain regions of the male brain, the male exhibits a bisexual orientation (13, 14). The *tra* gene also affects downstream sex-determination genes like *fruitless* and *doublesex*, which in turn control the sex pheromones or the male sexual orientation (15). Here, we expressed the *UAS-tra* transgene at different stages of development and in a particular group of abdominal cells, with the aim of producing a male fly with an unaltered sexual orientation, but with a female pheromonal profile.

To assess the critical period during which the *tra* gene product regulates pheromone expression, we transiently expressed *UAS-tra* throughout the organism at different developmental stages by crossing it to a line in which *GAL4* is fused to a *heat shock* 70 promoter (16). The *tra* gene, fused to a promoter containing a *GAL4*-dependent upstream activation sequence (*UAS*), was therefore expressed with the same temporal

Fig. 1. Production of sex pheromones in 4-day-old male flies as a function of temporal activation of *UAS-tra* or of *UAS-lacZ*. A single pulse of heat shock (37°C) was applied for 2 hours, at various times (or 6 hours before pupariation). Each data point represents the mean percentage (\pm SE) of 7-monoenes (%7-T + %7-P) and of 7,11 dienes (%7,11-HD + %7,11-ND) for 20 *hsp-GAL4 UAS-tra* individuals and for 10 *hsp-GAL4 UAS-lacZ* individuals. Control, non-heat-shocked *hsp-GAL4 UAS-tra* and *hsp-GAL4 UAS-lacZ* males yielded 52.8 ± 1.5 and $57.5 \pm 2.3\%$ 7-monoenes, and 0.9 ± 0.5 and 0% 7,11 dienes, respectively. Values were measured as in (21).



J.-F. Ferveur, F. Savarit, G. Sureau, J.-M. Jallon, Mécanismes de communication, Unité de Recherche Associée-CNRS 1491, Bâtiment 446, Université Paris-Sud, 91405, Orsay-Cedex, France.

C. J. O’Kane, Department of Genetics, University of Cambridge, Downing Street, Cambridge CB2 3EH, UK. R. J. Greenspan, Department of Biology and Center for Neural Science, New York University, 1009 Main Building, Washington Square, New York, NY 10003, USA.

*To whom correspondence should be addressed. E-mail: ferveur@ext.jussieu.fr

†Present address: The Neurosciences Institute, 10640 John Jay Hopkins Drive, San Diego, CA 92121, USA.